Available online at www.sciencedirect.com

ScienceDirect

journal homepage: www.elsevier.com/locate/he

# Structural and hydrogen absorption/desorption properties of $Zr_2(Co_{0.5}Fe_{0.2}Ni_{0.2}V_{0.1})$ intermetallic alloy

M. Komeili [a], H. Arabi [a,b,*], R.V. Yusupov [c], S.R. Ghorbani [b], F.G. Vagizov [c], F. Pourarian [d]

[a] Renewable Energy, Magnetism and Nanotechnology (REMAN) Research Laboratory, Faculty of Science, Ferdowsi University of Mashhad, Mashhad, Iran

[b] Department of Physics, Faculty of Science, Ferdowsi University of Mashhad, Mashhad, Iran

[c] Institute of Physics, Kazan Federal University, Kremlevskaya 18, 420008 Kazan, Russia

[d] Department of Materials Science and Engineering, Carnegie Mellon University, Pittsburgh, PA, USA

## HIGHLIGHTS

- $Zr_2(Co_{0.5}Fe_{0.2}Ni_{0.2}V_{0.1})$ intermetallic alloy is prepared by vacuum arc-melting method.
- This alloy has a multi-phase crystal structure with at least two different positions for iron atoms.
- High hydrogen capacity (2.1 wt%) and fast absorption kinetics (less than 100 s) are interesting features of this alloy.
- In the first three cycles, the maximum absorption capacity reduces about 25% and remains constant after that.
- This alloy has good anti-disproportionation behavior at least up to 8 bar and temperature lower than 783 K.

## GRAPHICAL ABSTRACT

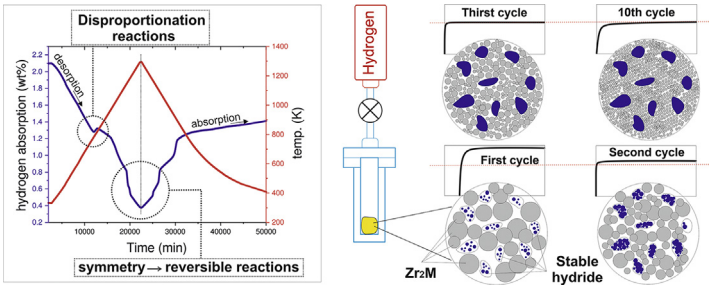


## ARTICLE INFO

*Article history:*
Received 6 October 2020
Received in revised form
31 January 2021

## ABSTRACT

The $Zr_2(Co_{0.5}Fe_{0.2}Ni_{0.2}V_{0.1})$ intermetallic alloy was prepared by arc melting method and its physical properties and hydrogen storage performance were investigated. XRD analysis by Rietveld refinement and Mössbauer spectroscopy measurements revealed a multiphase crystal structure, in which the dominant phases are C16 Laves phase. The hydrogen-induced cracks, chemical composition, and elements distribution were analyzed by SEM

* *Corresponding author*. Renewable Energy, Magnetism and Nanotechnology (REMAN) Research Laboratory, Faculty of Science, Ferdowsi University of Mashhad, Mashhad, Iran.
E-mail address: arabi-h@um.ac.ir (H. Arabi).

https://doi.org/10.1016/j.ijhydene.2021.03.045



Please cite this article as: Komeili M et al., Structural and hydrogen absorption/desorption properties of $Zr_2(Co_{0.5}Fe_{0.2}Ni_{0.2}V_{0.1})$ intermetallic alloy, International Journal of Hydrogen Energy, https://doi.org/10.1016/j.ijhydene.2021.03.045

Accepted 6 March 2021
Available online xxx

*Keywords:*
Activation parameters
Anti-disproportionation
Hydrogen absorption
$^{57}$Fe Mössbauer
Hydrogen kinetics
$Zr_2(Co_{0.5}Fe_{0.2}Ni_{0.2}V_{0.1})$ alloy

and EDX mapping. The optimum conditions for the activation process, hydrogen absorption kinetics, cyclic durability performance, and disproportionation behavior were discussed. $Zr_2(Co_{0.5}Fe_{0.2}Ni_{0.2}V_{0.1})$ alloy has a high absorption kinetic rate, with an activation energy of 10.11 kJ/mol, high hydrogen capacity (2.1 wt%) at room temperature, and good anti-disproportionation behavior (hydrogen pressure up to 8 bar and temperature below 783K). The hydrogen capacity decreased in the first three cycles (~25%) and then remained almost stable, which is likely caused by the high stability of hydride. The studied hydride has interesting features that can be considered for practical applications.



## Introduction

One of the most crucial challenges in using "Hydrogen as a fuel" in onboard applications is to store them safely and securely. For many years, scientists in the field of hydrogen storage have been trying to introduce and characterize some new materials for improving their hydrogen absorption and desorption properties. High capacity for absorbing hydrogen, operating at near ambient temperature and pressure, high absorbing/desorbing cycle durability, fast kinetic, and low cost of material are the most important parameters for a good hydrogen storage candidate. Intermetallic alloys are one of the best and well-known materials for hydrogen storage. High volume storage capacity, easy activation, high cyclic life, fast kinetic, and tunable absorption/desorption temperature and pressure by using elemental alloying or other common techniques are individual features of intermetallic alloys. However, a typical low gravimetric storage capacity (usually lower than 2 wt%) is the major drawback of them [1–3]. In addition, intermetallic alloys are used for non-storage applications include nickel-hydride battery, some thermal systems, purification hydrogen system, hydrogen sensor, and catalytic application [4–7].

Depending on the structure types and constituent elements, intermetallic alloy materials classify into several group families, namely $AB_5$, AB, $AB_2$, $AB_3$, and $A_2B$. In the $A_2B$ type family, A is an alkaline earth metal and B is a transition metal. Zirconium can be placed instead of A in this type of alloys. Zirconium has a larger atomic radius compared with the hydrogen atom, and it has a high affinity to react with hydrogen. Therefore, zirconium-based alloys have interesting properties regarding hydrogen storage. For example, these alloys usually have a very low plateau pressure for absorbing hydrogen [8,9]. So, they have not attracted much attention to the onboard applications. Nevertheless, this feature causes the Zr-based alloys considered as a great candidate for trapping tritium in the light water reactor for the fuel cladding. Non-radioactivation and low pyrophoricity nature, lower price, and high dissociation pressure at moderate temperatures are the advantages of using Zr-based alloys instead of uranium in storage and delivery hydrogen isotope [10]. Another application of these compounds is in ultra-high vacuum (UHV) systems as a "getter" for residual hydrogen in the vacuum chamber [11].

ZrCo alloy from the AB family type is a good candidate for fuel cladding [10]. However, the disproportionation reaction causes the formation of stable hydride phases, at a temperature above 573 K, resulting in limitation of desorption kinetic and consequently degradation of cycle life. In order to improve the kinetic performance of ZrCo, it is possible to decorate the particles of the alloy with catalytic elements such as nickel or modifying composition by elemental substitution [10]. The effect of decorating or substituting Ni and Fe instead of Co on ZrCo alloy has been investigated [12–15]. Nickel in $ZrCo_{1-x}Ni_x$ compound plays a catalytic role in decomposing molecular hydrogen bonds and simultaneously improves the hydrogen absorption kinetics. Furthermore, the addition of nickel content decreases the hydrogen desorption pressure (without any changing the storage capacity) and improves the cyclic stability of the ZrCo hydride [13,15]. On the other hand, the iron substitution in ZrCo leads to higher durability of the alloy against disproportionation reaction and consequently increases cyclic stability significantly [14]. Based on theoretical results, the restraint or acceleration of the disproportionation reaction by elemental substitution is attributed to the change in the Zr–H(8e) bond length or the size of the 8e site in ZrCo alloy [16]. Vanadium is another useful element that is added to the alloy for improving the hydrogen absorption kinetics [17]. Although vanadium plays a significant catalytic role in hydrogen storage reaction, it is an expensive element and increases the final cost of the alloy.

In spite of the fact that the binary ZrCo alloy is a good getter for tritium absorption, the $A_2B$ family compounds in the form of $Zr_2Co$ seems to be more suitable because the hydrogen absorption pressure is lower than in this compound. Furthermore, the compound in the form of $Zr_2M$ (M = Co, Ni, and Fe) have the highest H per atom (H/M = 5) among the other zirconium-based alloys [18]. The destructive phenomenon of disproportionation also occurs for this class of alloys. It is well known that high temperature, high hydrogen pressure, and repeated hydrogen absorption/desorption cycles are the three main factors that affect disproportionation reaction in Zr-based alloys [19]. The hydrogen-induced disproportionation mechanism in $Zr_2M$ (M = Co, Ni, and Fe) has been systematically investigated as a function of temperature. These binary alloys rapidly decompose into more stable phases at elevated temperatures of 773 K, and the stability order is reported as $Zr_2Ni > Zr_2Co > Zr_2Fe$ [20]. It was found that $Zr_2Co$, $Zr_2Ni$, and $Zr_2Fe$ binary alloys are highly sensitive to temperature and hydrogen pressure and quickly decomposed to stable phases [21–24]. Based on in-situ neutron diffraction data, $Zr_2FeH_5$ hydride decomposes to $ZrH_2$ at a temperature above 653 K and

Please cite this article as: Komeili M et al., Structural and hydrogen absorption/desorption properties of $Zr_2(Co_{0.5}Fe_{0.2}Ni_{0.2}V_{0.1})$ intermetallic alloy, International Journal of Hydrogen Energy, https://doi.org/10.1016/j.ijhydene.2021.03.045

decomposes to $ZrFe_2$ and $Zr_3Fe$ by increasing temperature above 803 K [23]. On the other hand, the initial pressure of hydrogen higher than 1 bar also causes the formation of $ZrH_2$ and the reduction of hydrogen absorption capacity in the $Zr_2Fe$ alloy [24].

In this study, the zirconium-based alloy in the form of $A_2B$ fabricated with the stoichiometric formula $Zr_2(Co_{0.5}Fe_{0.2}Ni_{0.2}V_{0.1})$ and measured some of its physical properties including structural and morphological properties. The local electronic environment of iron nuclei was studied by Mössbauer spectroscopy. It was found that the addition of iron, nickel, and vanadium improve the hydrogen storage properties. Some hydrogen storage properties such as activation behavior, cyclic durability performance, and hydrogenation kinetics were investigated in the temperature range of 273–795 K. Furthermore, the effect of temperature and pressure on disproportionation reaction are discussed.

## Experimental

The initial cobalt, iron, and nickel ingot with 99.9% purity and zirconium ingot with 99.5% purity were purchased from commercial sources and used without any further purification. The vanadium source was used in the powder form with 99.98% purity. Vanadium powder was first converted to a tablet inside an argon atmosphere glove box (for preventing oxidation) and then used as one of the starting materials. The materials were cut and weighed carefully to produce a 20 gr alloy with the stoichiometric ratio of $Zr_2(Co_{0.5}Fe_{0.2}Ni_{0.2}V_{0.1})$. The alloy fabricated by a vacuum arc-melting furnace (FZKH 100VAR H, Iran) on a water-cooled copper hearth. The chamber was flushed three times with argon gas (99.9999% purity) and then evacuated by a rotary and diffusion pump combination to provide a vacuum pressure of $5 \times 10^{-5}$ mbar. A titanium getter was used for removing any amount of residual oxygen in the chamber. The process of melting and re-melting was carried out five times in a suitable manner to ensure the homogeneity of the alloy composition.

The inductive coupling plasma (ICP) spectra of the alloy confirm that the stoichiometric ratio is correct. X-ray diffraction, SEM & EDX, and Mössbauer spectroscopy were used to examine the structural and morphological properties of the alloy composition. Hydrogenation properties of the alloy were measured by a home-made Sievert apparatus.

## Result and discussion

### *Characterization $Zr_2(Co_{0.5}Fe_{0.2}Ni_{0.2}V_{0.1})$ alloy*

Scanning electron microscopy (SEM) with energy dispersive X-Ray (EDX) system, (1450VP Leo, Germany), were used to identify the distribution of elements and quantify the elemental composition of the alloy. Fig. 1-a shows the general backscatter electron image (BEI). Fig. 1b–f demonstrate the EDX mapping images for cross-section of the $Zr_2(Co_{0.5}Fe_{0.2}Ni_{0.2}V_{0.1})$ sample for V, Fe, Co, Ni, and Zr elements, respectively. In the BEI results, a multiphase structure is obviously observed by distinguishing light gray, medium gray, and dark gray areas. By comparing Fig. 1-a and f, the EDX analysis shows that the medium gray area is zirconium rich. In these areas, the amounts of other elements are very low, which confirms that zirconium is not fully incorporated with other elements. Vanadium has precipitated in dark gray areas (compare Fig. 1a, and -b). In these areas, there are also iron, nickel, and cobalt, whereas the iron content is higher than Co and Ni (Fig. 1c–e). Zirconium content in the dark gray areas is much lower than in another one, which suggests dark areas are a mix of all elements, but the content of iron and vanadium are higher. The light gray area is homogeneously composed of all elements except vanadium.

Table 1 shows the elemental composition analysis of the sample. It was found that the theoretical composition supports the experimental results.

The crystal structure of the samples was investigated by X-ray diffractometer (BRUKER D8, Germany). Fig. 2 shows the X-ray diffraction patterns of the $Zr_2(Co_{0.5}Fe_{0.2}Ni_{0.2}V_{0.1})$ sample named "as-cast sample". The visual inspection of Fig. 2 reveals that the as-cast sample has a multiphase structure. In the multiphase alloy, precise phase identification is very difficult or maybe impossible because some peaks are superimposed by peaks of two or more phases. Therefore, Rietveld refinement analysis was applied for identification type, amount, and the number of phases. The refinement method was carried out based on the method proposed by Ref. [25] and by using FullProf software [26]. The content of each phase, final weighted average Bragg R-factor, and final reduced $chi^2$ are summarized in Table 2. The small value of fitting parameters indicates that the phase identification in the sample is acceptable.

The Rietveld analysis of the as-cast sample confirms that there are several phases, in which the dominant phases are $Zr_2Fe$, $Zr_2Co$, and $Zr_2Ni$ with the $CuAl_2$ (C16 Laves phase)-type structure (The total content of the C16 phases is about 79 wt %). The presence of C16 Laves phases was predicted in the composite structure, where they were highly presented in the Zr-rich sections of their ternary phase diagram [27,28]. Several small peaks at $2\theta = 34.3°$, 38.5°, and the shoulder at 34.8° are attributed to the formation of orthorhombic $Zr_3Co$ phase. Since the cobalt content in the alloy composite is higher than that of the other elements, $Zr_3Co$ phase is more likely to form than $Zr_3Fe$ or $Zr_3Ni$. The hexagonal Zr phase is also observed, indicating that part of the zirconium has not been incorporated into the final synthesized alloy composition. Already some zirconium regions were also observed in the EDX mapping spectra. The peak around $2\theta = 41°$ corresponds to the vanadium phase with a cubic structure. Probably, some zirconium and vanadium atoms in solid solution phases are generated during a fast and non-equilibrium solidification

**Table 1 – The average concentration of elements in the composition of $Zr_2(Co_{0.5}Fe_{0.2}Ni_{0.2}V_{0.1})$ from the EDX mapping analysis.**

| | Content/wt.% | | | | |
|---|---|---|---|---|---|
| | Zr | Co | Ni | Fe | V |
| Experimental | 76.93 | 11.97 | 4.81 | 4.43 | 1.86 |
| Theoretical | 76.29 | 12.27 | 4.89 | 4.42 | 2.12 |

Please cite this article as: Komeili M et al., Structural and hydrogen absorption/desorption properties of $Zr_2(Co_{0.5}Fe_{0.2}Ni_{0.2}V_{0.1})$ intermetallic alloy, International Journal of Hydrogen Energy, https://doi.org/10.1016/j.ijhydene.2021.03.045

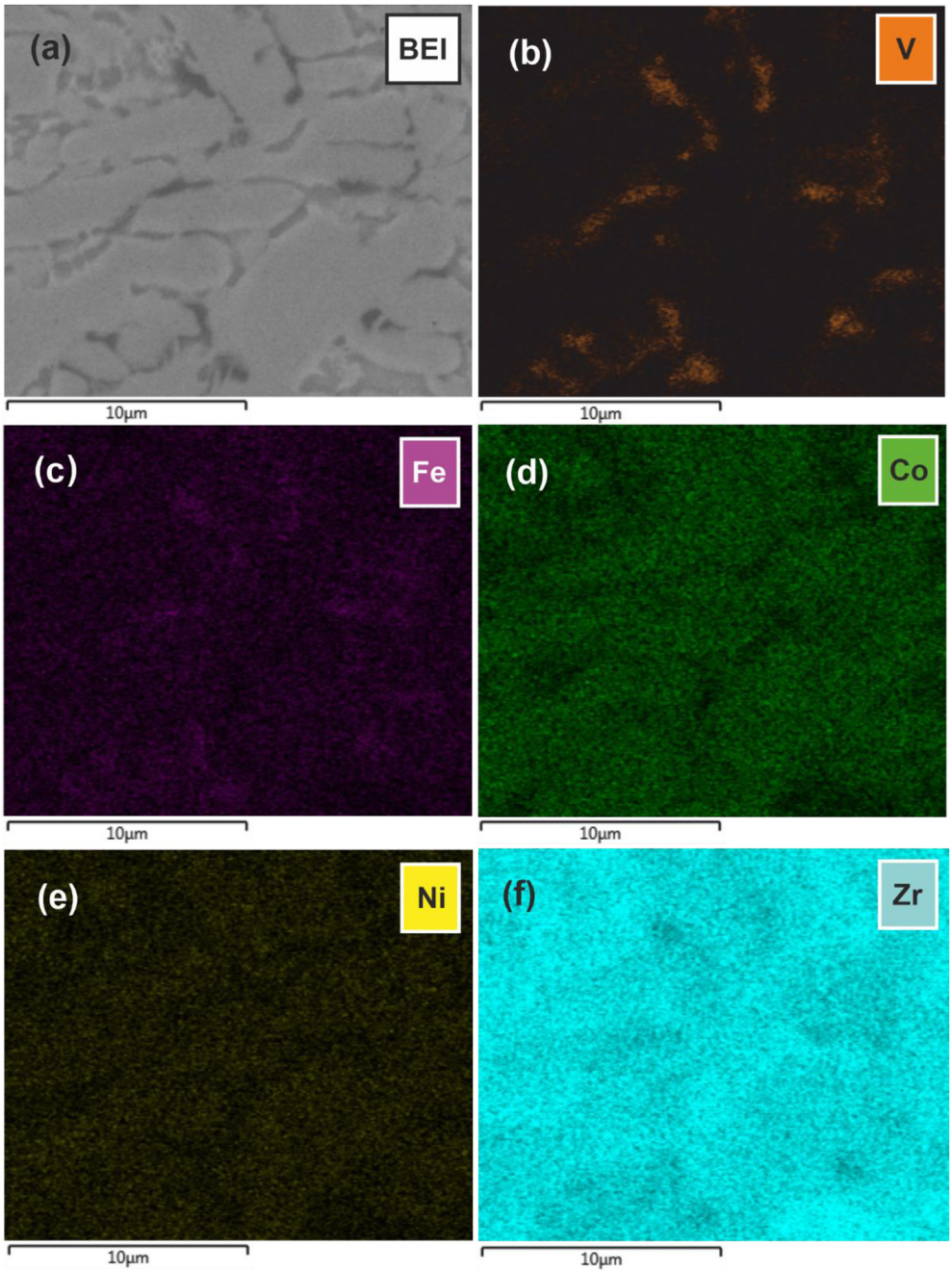


**Fig. 1 – Backscatter electron image and EDX mapping analysis of the $Zr_2(Co_{0.5}Fe_{0.2}Ni_{0.2}V_{0.1})$ alloy. Each element is marked with a specific color. The concentration of the elements is proportional to the color intensity associated with them. (For interpretation of the references to colour in this figure legend, the reader is referred to the Web version of this article.)**

process, and the annealing treatment at high temperature may be effective in eliminating them.

The Mössbauer spectroscopy (MS) was used to study the electronic environment and valence state of iron atoms. Mössbauer measurements have been done in a transmission geometry using a constant-acceleration spectrometer (Wissel, Germany). $^{57}$Fe source was Co-57 in rhodium matrix 35 mCi in activity. The best least-squares fit the Mössbauer spectra, by the assumption that line shapes are Lorentzian, yields values of the hyperfine parameters, namely isomer shift (IS) and quadrupole splitting (QS). Due to the little amount of iron in the alloy, each measurement took about two days for obtaining the desired signal to noise ratio. This sample shows paramagnetic like behavior at room temperature. Furthermore, any trace of magnetic hyperfine interaction was not detected by doing the measurement at 80 K.

The phase diagram of Zr–Fe compound illustrates several crystalline phases as follows: The most important of these phases are $Zr_2Fe$ with tetragonal body-centered structure (C16 Laves phase), $Zr_2Fe$ with cubic diamond structure, $Zr_3Fe$

Please cite this article as: Komeili M et al., Structural and hydrogen absorption/desorption properties of $Zr_2(Co_{0.5}Fe_{0.2}Ni_{0.2}V_{0.1})$ intermetallic alloy, International Journal of Hydrogen Energy, https://doi.org/10.1016/j.ijhydene.2021.03.045

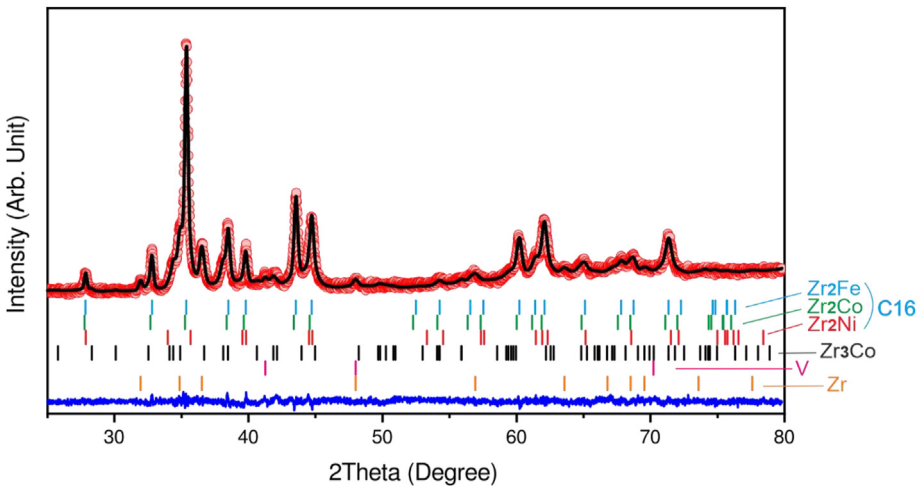


**Fig. 2 – X-ray patterns and its Rietveld refinement of $Zr_2(Co_{0.5}Fe_{0.2}Ni_{0.2}V_{0.1})$ alloy. Red points show the experimental XRD data. The black line is the calculated patterns that are obtained from Rietveld refinement. Colorful vertical bars show the positions of the Bragg peaks for each phase. The blue line shows the difference between the experimental XRD data and the calculated patterns. (For interpretation of the references to colour in this figure legend, the reader is referred to the Web version of this article.)**

having orthorhombic phase, $ZrFe_2$ and $Zr_6Fe_{23}$ with cubic structure and iron solid solution in alpha or beta zirconium phase [27–29]. According to the XRD results, it is favorable that the mixed substitution of cobalt, nickel, or both of them can take place in each structure of the phase diagram. Fig. 3 and Table 3 show the MS spectrum and parameters of the fitting for the as-cast sample, respectively. There are two quadrupole doublets, the first doublet with an isomer shift IS = −0.30 mm/s and quadrupole splitting QS = 0.70 mm/s ascribed to the tetragonal phase of $Zr_2Fe$ (C16) [30,31]. The second doublet has the following parameters: IS = −0.19 mm/s, QS = 0.15 mm/s. The line width of this doublet is almost 1.4 times wider than the lines of the first doublet. This observation is probably because, in addition to zirconium atoms other elements such as cobalt, nickel, or even vanadium atoms can be found in the nearest vicinity of the iron atom. Besides, the line broadening may be because this phase is poorly crystallized, and its reflections are not even visible in the X-ray diffraction patterns. One of the reasons may also be nano/micro clustering. If we compare the temperature change in the isomer shift (ΔIS) from room to liquid nitrogen temperature for the $Zr_2Fe$ phase, we see that for $Zr_2Fe$, ΔIS is 0.12(5) mm/s, and for the second phase, it is about 0.14 mm/s. This means that the Debye temperature for the second phase is noticeably lower than for $Zr_2Fe$. Therefore, the iron atoms in the second phase are bond more weakly to the surrounding atoms than for the $Zr_2Fe$ phase. Based on these data, we can assume that the second doublet may be related to the composition of the form $Zr_x(Fe, Co, Ni)_y$.

In general, the Fe isomer shift ($\delta_{Fe}$ = IS) is proportional to the s-electron density ρ(0) at $^{57}Fe$ nuclei, which in metals and alloys is mostly dependent on the 3d-electron shell configuration and s-electron band population of iron atoms. Usually, when the Fe atom is confined in a small volume, the s-electron density at its nucleus becomes larger, and the value of $\delta_{Fe}$ reduces. Therefore, the difference in IS values between $Zr_2Fe$ with IS = −0.30 mm/s and the second doublet (approximately IS = −0.19 mm/s) is considered to be due to the neighboring iron atoms. This is usually the case in Zr–Fe alloys, where a highly electronegative iron acquires electrons from electropositive zirconium. Such charge transfer determines very large negative values of $\delta_{Fe}$ for binary Zr–Fe compounds, such as tetragonal $Zr_2Fe$, where all the nearest neighbors of the iron atoms are zirconium atoms. Therefore, the X-ray and the Mössbauer measurements results show that the main iron-containing phase is the $Zr_2Fe$. Zirconium atoms have already been consumed to form the Zr-enriched phase. Therefore, the second phase (second doublet) can be of the type $Zr_x(Fe,Co,Ni)_y$, where y > x. This is also evidenced by the value of the isomer shift, a decrease in the number of zirconium atoms in the nearest vicinity of the iron atoms, and it led to a shift of the isomer shift toward positive values [32].

**Table 2 – The amount of each crystalline phase and the parameters of the fitting calculated from Rietveld refinement analysis. $R_{wp}$ = 12.6**

| Sample | Phase abundance (wt.%) | | | | | | Error | |
|---|---|---|---|---|---|---|---|---|
| | C16 Laves phase | | | | | | | |
| as-cast | $Zr_2Fe$ | $Zr_2Co$ | $Zr_2Ni$ | $Zr_3Co$ | Zr | V | Av.R–F[a] | $Chi^2$ |
| | 54.89 | 18.98 | 4.95 | 13.49 | 5.41 | 2.26 | 4.6 | 1.7 |

[a] Final weight av. Bragg R-Factor.

Please cite this article as: Komeili M et al., Structural and hydrogen absorption/desorption properties of $Zr_2(Co_{0.5}Fe_{0.2}Ni_{0.2}V_{0.1})$ intermetallic alloy, International Journal of Hydrogen Energy, https://doi.org/10.1016/j.ijhydene.2021.03.045

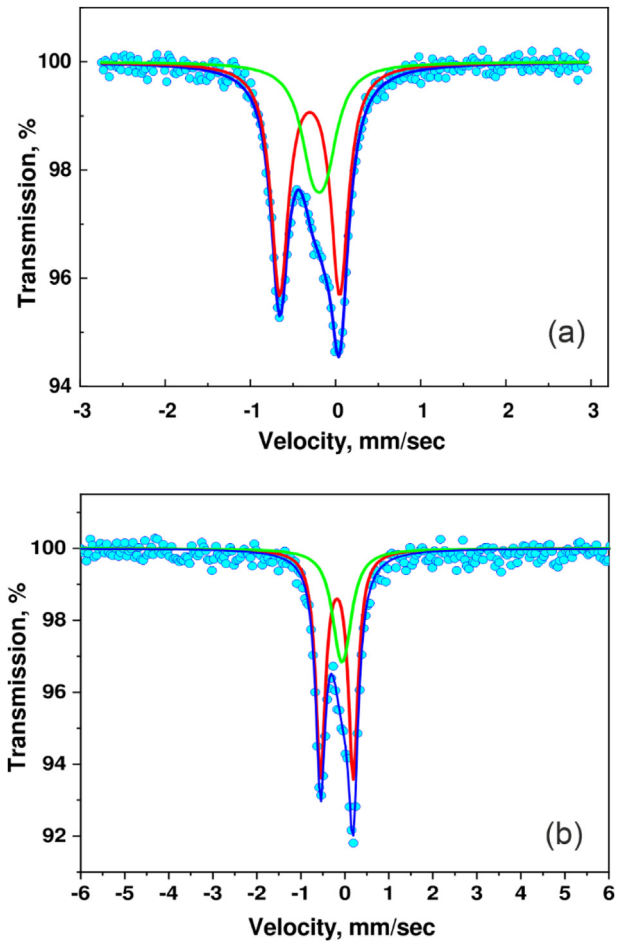


**Fig. 3 – Mössbauer spectra of $^{57}$Fe nuclei in the as-cast sample: a) at room temperature, b) 80K**

A value of QS is defined by the symmetry of the iron electron shells and local symmetry of the crystal lattice near the iron atom. In Zr–Fe alloys, for example in Zircaloys, the values of QS are large in tetragonal $Zr_2$(Ni, Fe) (C16), small in hcp Zr(Cr, $Fe)_2$ (C14), and even smaller in fcc Zr(Cr, $Fe)_2$ (C15) [33]. The electronic environment of iron atoms in the second phase is relatively symmetrical (QS = ~0.15 mm/s) which is possible when structural changes occur from the tetragonal type to the hexagonal cubic (C15) one. Taking into account that the Mössbauer parameters of Zr–Fe alloys depend on the synthesis conditions, composition, heat treatment, quenching, etc. Therefore, the parameters of the second doublet are in agreement with those addressed in the literature [31,34]. Thus, the second center for iron in the as-cast sample

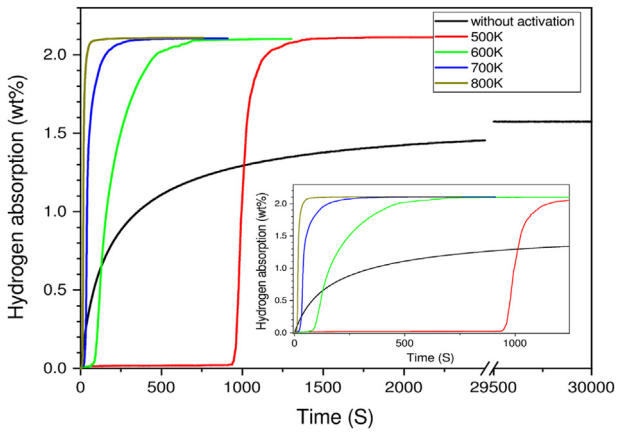


**Fig. 4 – Hydrogen absorption kinetic curve for samples without and with activation process at different temperature (kinetic curves measured at 2.65 bar hydrogen pressure after 30 min and room temperature).**

corresponds to poorly crystallized particles of the composition $Zr_x$(Fe, Co, $Ni)_y$, where y > x.

### *Optimization of activation parameters*

Finding the optimal condition for Zr-based alloy activation is essential for kinetic measurements. The kinetic property and hydrogenation parameters of these alloys, including maximum capacity, kinetics time for complete hydrogenation, and cycle durability, depend on activation conditions, which were intern drastically changed by phase separation and disproportionation effect.

Two experiments were designed to study the influencing parameters, including temperature and time of activation in the heat treatment. The first experiment is finding the optimal temperature in the heat treatment of the activation process. The sample was placed between two hardened steel plates and crushed into smaller pieces by a hydraulic press. Then, it was mechanically grounded well by using an agate mortar and pestle into a fine powder and passed through the sieve of 70 U S. Mesh. The powder does not react with oxygen under ambient conditions, so there is no need for an inert atmosphere glove box during powder preparation steps. 0.15 g of the powder was loaded into the reactor, and the system was washed three times with helium gas and then vacuumed continuously. The sample with no activation process is subjected to a hydrogen pressure of 2.65 bar until hydrogen absorption was stable. Other samples were heated at 500, 600,

**Table 3 – Parameters of Mössbauer spectra and their attributed phase.**

| Sample | | [a]IS(mm/s) | QS(mm/s) | Half Width | Composition | Phase name |
|---|---|---|---|---|---|---|
| as-cast at RT | Doublet1 | −0.30(3) | 0.70(5) | 0.24(9) | 67.(6)% | $Zr_2Fe$ |
| | Doublet2 | −0.19(3) | 0.15(5) | 0.34(4) | 32.(3)% | $Zr_x$(Fe,Co,Ni)$_y$, y > x |
| as-cast at 80K | Doublet1 | −0.18(1) | 0.74(4) | 0.26(4) | 67.(9)% | $Zr_2Fe$ |
| | Doublet2 | −0.06(3) | 0.13(5) | 0.45(2) | 32.(1)% | $Zr_x$(Fe,Co,Ni)$_y$, y > x |

[a] The isomer shifts are defined relative to iron metal.

Please cite this article as: Komeili M et al., Structural and hydrogen absorption/desorption properties of $Zr_2(Co_{0.5}Fe_{0.2}Ni_{0.2}V_{0.1})$ intermetallic alloy, International Journal of Hydrogen Energy, https://doi.org/10.1016/j.ijhydene.2021.03.045

700, and 800 K in the presence of a dynamic vacuum ($<10^{-2}$ mbar) for 30 min. After cooling downo room temperature, the powder was exposed to a hydrogen pressure of 2.65 bar. Fig. 4 shows the hydrogen absorption kinetics of the alloys activated at various temperature.

The sample without the activation process absorbed hydrogen immediately started after purging of $H_2$ gas and increased very slowly. The maximum capacity of this sample (1.57 wt%) reaches the lowest value among other samples even after a long time, which indicates the activation process is necessary for complete hydride formation. The maximum value of hydrogen capacity (2.1 wt%) is the same for all samples at various heating temperatures from 500 to 800 K in Fig. 4. Apart from that, $Zr_2(Co_{0.5}Fe_{0.2}Ni_{0.2}V_{0.1})$ alloy absorbed hydrogen after a delay time inversely proportional to the selected temperature of heat treatment.

The unusual results of the samples (the slow kinetics of hydrogen absorption and the lower value of the hydrogen capacity in the sample without activation and observing a delay time for heated samples) can be explained by two effects [35]: (1) The surface composition of Zr-based alloys is affected by temperature, which is described by "surface segregation". Surface segregation in this study refers to the difference in atomic concentration of zirconium and other 3d metals atom (Co, Ni, Fe, and V) in the surface and the bulk of the sample. This phenomenon is common to zirconium-based alloys [35,36]. Therefore, the atomic concentration of 3d metals on the surface particles is increased by increasing temperature, associated with enhanced catalytic activity for the adsorption of $H_2$ molecules in these metals. (2) The surface protective $ZrO_2$ layer is an effective barrier against hydrogen absorption. These layers are formed on the surface of Zr-based alloy because of the large negative free energy of its formation and can be gradually destroyed with the increase of temperature [35,37]. According to the presented data in Fig. 4, the optimum temperature of 700 K was selected for complete hydrogen absorption. The samples with the activation process pulverized by hydrogen absorption and converted to fine gray metallic powder due to a lattice volume expansion while no trace of this effect observed in the sample without activation. This observation can confirm that the hydrogen absorption in the sample without activation was not complete.

The second parameter for the activation process is time. To evaluate the effect of activation time on the hydrogen absorption kinetic curve, the powder, based on the last experiment, was heated to 700 K for 10 min to 3 h, and then cooled down to room temperature. By applying a hydrogen pressure of 2.65 bar, with the same conditions as the previous experiment, hydrogenation performed in a short time. Fig. 5 indicates the hydrogen absorption kinetic curve as a function of time for different preheated treatment time intervals. The maximum capacity of the hydrogen absorption is almost the same in all activation time. The time delay is reduced by increasing the activation times, which is clearly observed from the inset of Fig. 5. The time of activation has a significant influence on the delay time of hydrogen absorption and time of hydrogen saturation as reported in the literature as well as this study [35]. The reduction of hydrogen capacity for 3 h heat treatment is unknown for us. However, it can be seen that the maximum hydrogen capacities at various times of activation

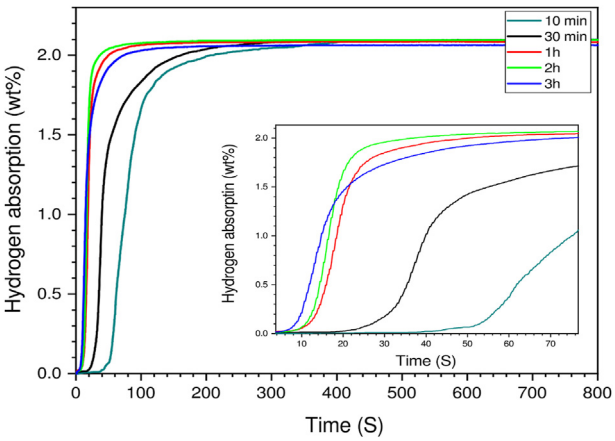


**Fig. 5 – Hydrogen absorption kinetic curve, which activated at 700 K, at various activation time (by applying 2.65 bar hydrogen pressure at room temperature).**

were very close to each other, suggesting that the effect of time activation is negligible. Therefore, the optimum activation time of 2 h was adopted in the subsequent experiments of this study.

One of the important parameters for the hydrogen absorption process is the amount of pressure applied to the sample as the driving force. In order to deduce the optimum pressure in the hydrogen absorption, heated powders at 700 K for 2h examine at different pressure, as shown in Fig. 6. No disproportionation reaction was observed up to hydrogen pressure of 8 bar, indicating that this alloy has relatively good resistance to the hydrogen pressure. As shown in the inset of Fig. 6, by increasing the applied hydrogen pressure, reaching maximum absorption occurs in a shorter time. This phenomenon can be predicted by increasing the driving force of the hydrogen on the structure of the alloy via increasing the applied hydrogen pressure. In fact, as the initial pressure during the hydriding reaction increases, the hydrogen concentration in the surface of the bulk increased, i.e. the driving force, which diffuses the hydrogen atoms into the bulk of the

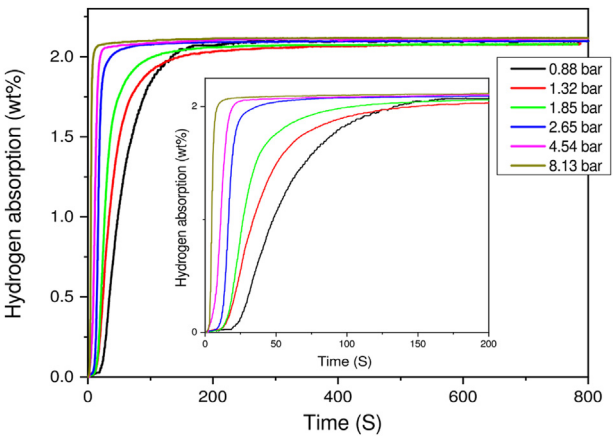


**Fig. 6 – The effect of applied hydrogen pressure on the absorption kinetics of $Zr_2(Co_{0.5}Fe_{0.2}Ni_{0.2}V_{0.1})$ alloy at room temperature.**

Please cite this article as: Komeili M et al., Structural and hydrogen absorption/desorption properties of $Zr_2(Co_{0.5}Fe_{0.2}Ni_{0.2}V_{0.1})$ intermetallic alloy, International Journal of Hydrogen Energy, https://doi.org/10.1016/j.ijhydene.2021.03.045

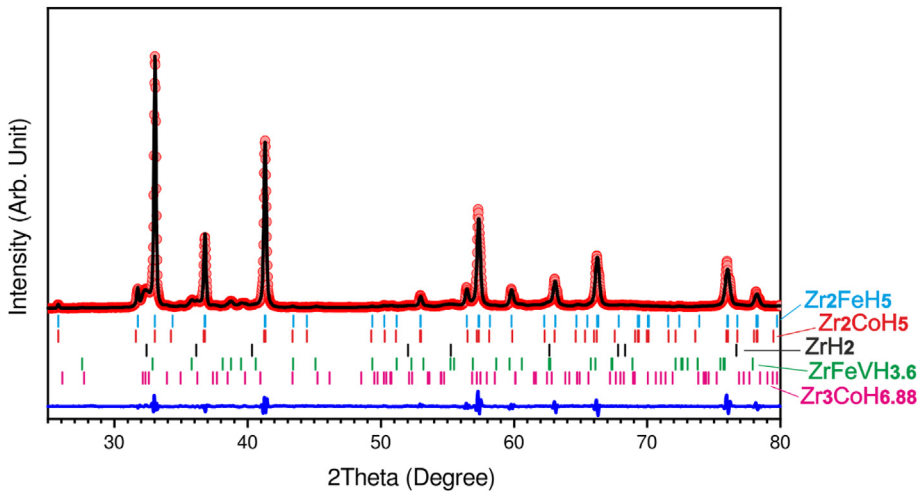


**Fig. 7 – X-ray patterns and its Rietveld refinement of $Zr_2(Co_{0.5}Fe_{0.2}Ni_{0.2}V_{0.1})$ alloy after hydrogenation. Red points show the experimental XRD data. The black line is the calculated patterns that are obtained from Rietveld refinement. Colorful vertical bars show the positions of the Bragg peaks for each phase. The blue line shows the difference between experimental XRD data and the calculated patterns. (For interpretation of the references to colour in this figure legend, the reader is referred to the Web version of this article.)**

sample, increases. Consequently, the activation energy decreases and the delay time of hydrogen absorption becomes shorter, associated with the faster reaction rate, which is consistent with the result of Fig. 6.

Fig. 7 shows the XRD patterns and Rietveld refinement of $Zr_2(Co_{0.5}Fe_{0.2}Ni_{0.2}V_{0.1})$ alloy after activation process with hydrogen at 2.65 bar, 2 h at 700 K. By comparing the XRD pattern of hydride sample with the as-cast one (that shown in Fig. 1), all the peaks of C16 Laves phases and Zr, $Zr_3Co$ and V phases have disappeared, and some new related hydride phases have formed. The main hydride phases correspond to the tetragonal $Zr_2MH_5$ (M = Co, Fe, or Ni) phase similar to an $Al_2Cu$-type metal atom arrangement. Based on the result of Rietveld refinement (Table 4), the tetragonal phases are the main crystalline phases with about 74 wt%. Furthermore, other hydride phases, including $ZrH_2$, $ZrFeVH_{3.6}$, and $Zr_3CoH_{6.6}$ phases, are identified in the XRD pattern. The hexagonal α-Zr and $Zr_3Co$ phases were previously observed in the XRD spectrum of the as-cast sample. These phases react with hydrogen to produce $ZrH_2$ and $Zr_3CoH_{6.6}$ phases with phase abundance of 11.15 and 3.89 wt%, respectively. $ZrFeVH_{3.3}$ phase is created in this sample, probably due to hydrogenation of $Zr_x(Fe, Co, Ni)_y$ phase, where $y > x$, which is mentioned in Mössbauer spectroscopy. The absence of ZrCo, ZrNi, and $ZrFe_2$ phases in the hydride sample indicates that the disproportionation reaction did not occur [13].

Fig. 8 illustrates the SEM micrographs of the $Zr_2(Co_{0.5}Fe_{0.2}Ni_{0.2}V_{0.1})$ alloy particles before and after the hydrogenation process at different magnifications. In the as-cast sample, SEM images revealed a brittle fracture surface. Hydrogenation is led to the appearance of some micro crack in the surface of the alloy, which can be attributed to the expansion of lattice parameters due to the hydrogen absorption process.

### *Cyclic durability*

The powder of $Zr_2(Co_{0.5}Fe_{0.2}Ni_{0.2}V_{0.1})$ submitted to hydrogen at the pressure of 2.65 bar after activating process until the hydride formation in the alloy is completed. In the first cyclic test, excess hydrogen was removed from the hydride-containing reactor by a vacuum pump. The hydride heated through a programmable oven up to 840 K with the heating rate of 5 K/min and then cool down to room temperature. The changes in stored hydrogen in the alloy were recorded and cyclic tests, as described above, were performed for ten absorption/desorption cycles (as shown in Fig. 3). It is observed that the hydrogen capacity in the first cycle is decreased from 2.1 to 1.3 wt% as temperature increased. During the cooling step, the sample reabsorbs hydrogen up to 1.6 wt%.

The capacity variation during the second cycle significantly decreases (less than 8%) from the first one and remains almost constant in the third cycle and after that.

**Table 4 – The amount of each crystalline phase and fitting parameters from Rietveld refinement analysis. $R_{wp} = 9.89$**

| sample | Phase abundance (wt.%) | | | | | Error | |
|---|---|---|---|---|---|---|---|
| Main phase | | | | | | | |
| Hydrogenation sample | $Zr_2FeH_5$ | $Zr_2CoH_5$ | $ZrH_2$ | $ZrFeVH_{3.6}$ | $Zr_3CoH_{6.88}$ | Av.R–F[a] | $Chi^2$ |
| | 55.50 | 18.68 | 11.15 | 10.78 | 3.89 | 2.5 | 2.3 |

[a] Final weight av. Bragg R-Factor.

Please cite this article as: Komeili M et al., Structural and hydrogen absorption/desorption properties of $Zr_2(Co_{0.5}Fe_{0.2}Ni_{0.2}V_{0.1})$ intermetallic alloy, International Journal of Hydrogen Energy, https://doi.org/10.1016/j.ijhydene.2021.03.045

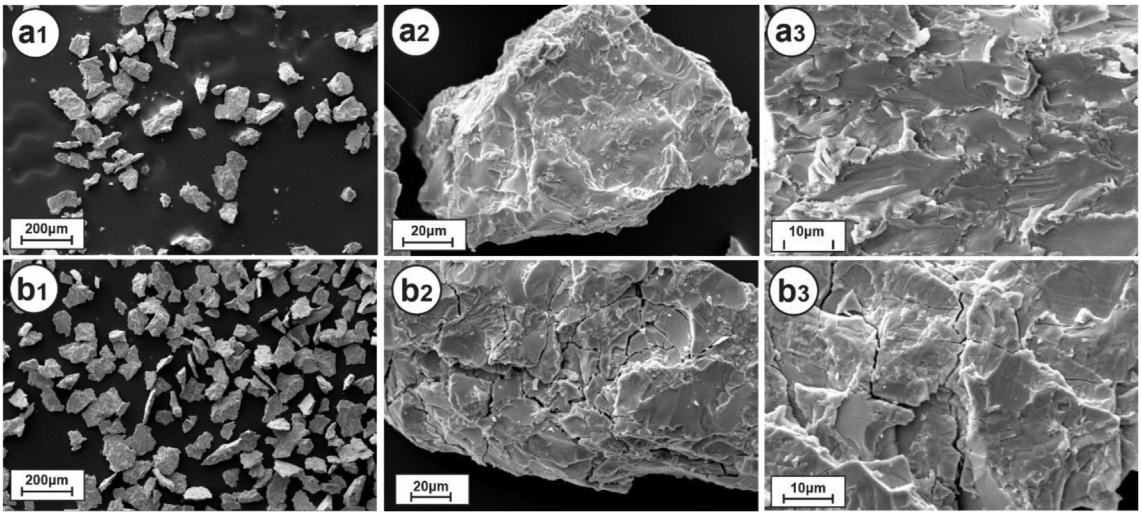


**Fig. 8 – SEM micrographs of the $Zr_2(Co_{0.5}Fe_{0.2}Ni_{0.2}V_{0.1})$ alloy particles (a) as-cast (b) hydrogenation sample.**

In order to gain a better insight into the capacity degradation in the initial cycles, consecutive absorption kinetic measurements were performed. The desorption step for each kinetic curve was carried out at 700 K for 2h under a dynamic vacuum, as explained in the activation section. The result is presented in Fig. 9. In the first cycle, the hydrogen absorption starts after an incubation period time of about 12 s and reaches 2.1 wt% as the maximum hydrogen capacity after about 2 min. The second absorption takes place without any delay time and reaches a saturation value (1.73 wt%) in 38 S, showing a very fast kinetic absorption behavior of this activated material. The capacity reaches 1.6 wt% in the third cycle, and the kinetic of absorption in this cycle is as fast as for the second cycle. At the higher cycles, the capacity reached an almost stable value of about 1.58 wt%.

The reduction of hydrogen capacity in the first cycles can be of several reasons: First, zirconium-base alloys have a high affinity for hydrogen absorption and therefore inherently very stable. For instance, the plateau pressure of hydrogen absorption is less than 0.1 atm in most of these alloys [8,9,18], and complete hydrogen desorption is not possible without applying high temperatures and high vacuum pumping. Second, disproportionation reaction and degradation of zirconium alloys are common phenomena in these types of alloys that lead to forming highly stable phases and non-absorbing compounds [18,20].

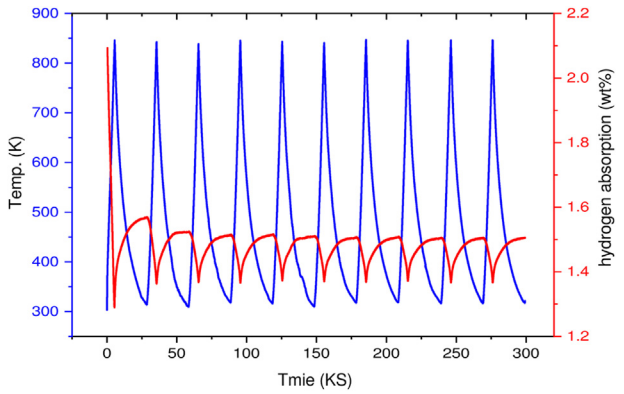


**Fig. 9 – Hydrogen absorption/desorption content as temperature changes during 10 cyclic measurements.**

Fast kinetics of hydrogen absorption in the second and higher cycles is ascribed to reducing the particle size. Hydrogen absorption and desorption cause cracking in the surface area of particles due to the expansion and contraction of the lattice parameter. As the particle size decreases, the surface area of the alloy increased, and subsequently, hydrogen penetrates more easily into the alloy [38]. At the higher cycles, reaching a maximum absorption takes place in a longer time, while the maximum absorbed hydrogen value is almost the same (ref. Fig. 10). In fact, the smaller particle size and pulverization deteriorated the heat and mass transfer during absorption and consequently decreased the kinetic performance [39].

XRD profiles after 2, 4, and 6 cycles of hydrogen absorption/desorption kinetics are shown in Fig. 11. The hydride phase ($Zr_2MH_5$ M = Co or Fe) having tetragonal symmetry appears in all cycles. The diffraction peaks of this phase became sharper and shifted to the higher angles with more absorption/desorption cycle, indicating that the crystal structure of this phase is refined and the sample more pulverized.

In addition to $Zr_2MH_5$ with tetragonal symmetry as the main phase, some peaks assigned to the secondary phases such as $ZrH_2$, $ZrFeVH_{3.6}$, and $Zr_3CoH_{6.6}$ found in the XRD pattern. The intensity of these phases ($2\theta = 32.14, 34.9, 38.6$) increased from the second cycle to the fourth cycle and then remained almost unchanged. By considering this fact and also the stability of the maximum hydrogen capacity after fourth absorption/desorption cycles, as shown in Fig. 10, it may be concluded that the generation of these secondary phases is responsible for the degradation of hydrogen capacity. Among the stable phases, $ZrH_2$ is a highly stable phase that decomposes at temperatures above 973 K [40]. Another hydride phase based on Zr–V is also a stable phase that adding Fe atom to its structure (in our case $ZrFeVH_{3.6}$) facilitates the release of

Please cite this article as: Komeili M et al., Structural and hydrogen absorption/desorption properties of $Zr_2(Co_{0.5}Fe_{0.2}Ni_{0.2}V_{0.1})$ intermetallic alloy, International Journal of Hydrogen Energy, https://doi.org/10.1016/j.ijhydene.2021.03.045

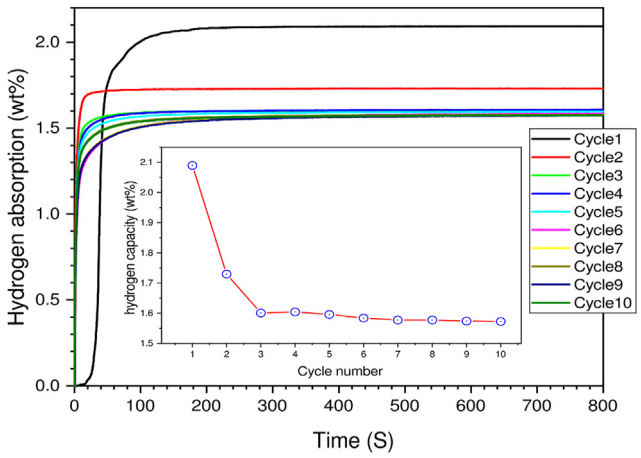


**Fig. 10 – Hydrogen absorption kinetic curves of the sample during 10 cyclic tests. Inset: the variation of maximum capacity during 10 absorption/desorption cycles.**

hydrogen and reducing the stability of the hydride phase in the sample [41]. The hydrogen stored in these phases cannot be desorbed in our experimental conditions ($<10^{-2}$mbar and 700 K). Therefore, degradation of hydrogen capacity could be observed. The stability of hydrogen absorption capacity after fourth cycles and absence of $ZrM_2$ phases (M = Co, Ni, and Fe) in XRD patterns, clearly indicating that $Zr_2(Co_{0.5}Fe_{0.2}Ni_{0.2}V_{0.1})$ alloy is a valuable candidate for anti-disproportionation properties which is fantastic for application.

### *Kinetic curve and activation energy*

The first hydrogen absorption kinetics of the sample was carried out at different operating temperatures from 273 K to 795 K after the same complete activation process (2 h at 700 K). The maximum hydrogen capacity decreases almost linearly by increasing the temperature from 2.1 to 1 wt%, as shown in Fig. 12. This effect can be attributed to the reversible absorption/desorption of hydrogen from the alloy surface [38]. The reaction kinetics of $Zr_2(Co_{0.5}Fe_{0.2}Ni_{0.2}V_{0.1})$ alloy was analyzed using different kinetic models [42] and the method described by Ref. [43]. The kinetic data were recorded after three absorption/desorption cycles to minimize the effects of particle size distribution and surface protective layers on the particles. Hydrogen immediately penetrates the alloy without any incubation time. The nature of the kinetic curves in all temperatures (Fig. 12(b)) is similar, but the time for reaching the saturation is shorter at elevated temperature, as expected. Fig. 12(b) shows the hydrogenation reacted fraction (ζ) as a function of time. The reacted fraction, ζ, is obtained from the ratio $(P-P(t))/(P-P_\infty)$, where P, P(t) and $P_\infty$ are the initial pressure of the reaction, the pressure at reaction time t and at final equilibrium, respectively. The experimental kinetic data can be described successfully by a second-order reaction kinetics equation [44]:

$$(1/(1-\zeta)) - 1 = kt \quad (1)$$

where k is the reaction rate constant. The plots of (1/(1-ζ))-1 versus t at different temperatures and their linear fits are shown in Fig. 12 (c). The values of the goodness of the fit ($R^2$ correlation coefficient), are very close to 1, which indicates that this model is suitable for the description of hydrogen absorption kinetics of $Zr_2(Co_{0.5}Fe_{0.2}Ni_{0.2}V_{0.1})$ alloy. In the second-order reaction model, the kinetic reaction is supposed to be simple and homogeneous and the reaction rate is proportional to the square of the concentration of absorbent [44].

The apparent activation energy ($E_a$) for a typical hydrogen kinetic reaction can be determined using the Arrhenius plot [ln(k) vs. 1000/T], as presented in Fig. 12 (d).

The activation energy of hydrogen absorption has been found to be 10.11 kJ/mol.

Comparing this value with the activation energy of the standard alloys and some other alloys (Table 5) shows that the energy required to start the hydrogen reaction in $Zr_2(Co_{0.5}Fe_{0.2}Ni_{0.2}V_{0.1})$ alloy is low, and, as a result, the kinetics of hydrogen absorption is very fast, as experimentally observed.

### *Temperature dependence and disproportionation effect*

The final experiment was carried out to find the hydrogen desorption behavior of $Zr_2(Co_{0.5}Fe_{0.2}Ni_{0.2}V_{0.1})$ alloy at high temperatures. One aspect of this experiment was finding the

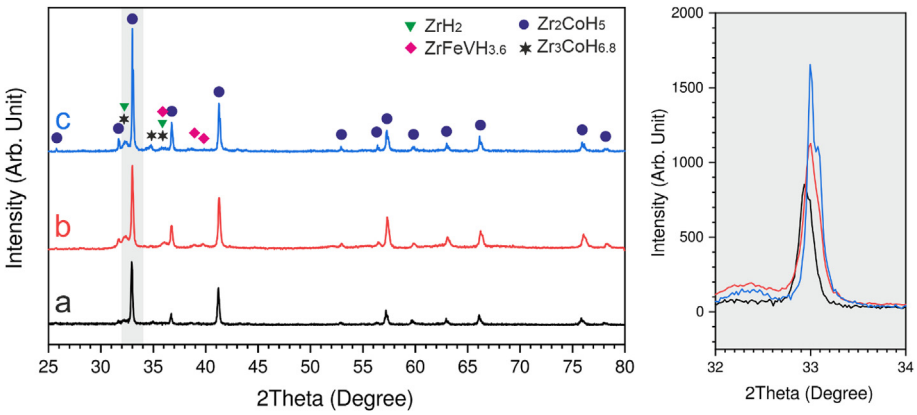


**Fig. 11 – XRD patterns of the $Zr_2(Co_{0.5}Fe_{0.2}Ni_{0.2}V_{0.1})$ alloy a) after 2 cycles, b) after 4 cycles and c) after 6 absorption/desorption cycles at room temperature.**

Please cite this article as: Komeili M et al., Structural and hydrogen absorption/desorption properties of $Zr_2(Co_{0.5}Fe_{0.2}Ni_{0.2}V_{0.1})$ intermetallic alloy, International Journal of Hydrogen Energy, https://doi.org/10.1016/j.ijhydene.2021.03.045

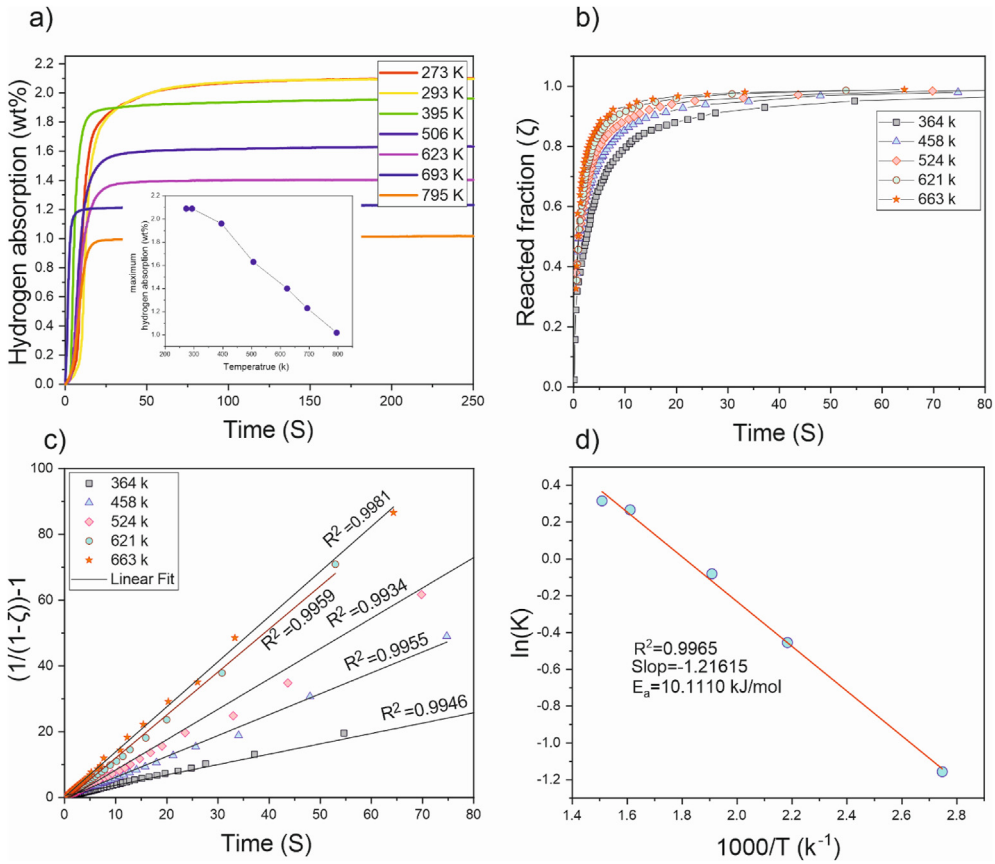


**Fig. 12 – a) the first hydrogen absorption kinetics of $Zr_2(Co_{0.5}Fe_{0.2}Ni_{0.2}V_{0.1})$ alloy at various temperatures after subjecting 2.65 bar hydrogen pressure, Inset: The value of maximum hydrogen capacities versus temperature. b) Kinetics of hydriding reaction after three absorption/desorption cycles. c) Plots of [1/(1-ζ)-1] vs. time for hydriding reaction at various temperatures and their linear fits. d) calculation of apparent activation energy.**

temperature dependence of the disproportionation phenomenon. In order to reach this goal, we modified our homemade apparatus by replacing a quartz tube reactor instead of the stainless steel one because of heating the sample to 1300 K. A thermocouple type-k, fixed on the end of the quartz tube for measuring the local temperature around the sample instantaneously. After the activation process, the hydrogen was gradually injected into the reactor until the alloy is completely hydride at room temperature. The hydride was heated up to 1300 K and then cooled down to room temperature at a rate of 5 K/min heating and cooling rate.

Fig. 13 represents, in a double-Y plot, the hydrogen desorption of hydride and the temperature of the sample and time elapsed since the start of the experiment. The amount of hydrogen inside the sample began to drop immediately after starting the heating process and it decreased almost linearly with temperature until reached T = 783 K. After that, the hydrogen capacity increases slightly up to 825 K and then decreases again. This behavior is probably related to the disproportionation reaction between $A_2B$ phases ($Zr_2Co$, $Zr_2Ni$, and $Zr_2Fe$) and hydrogen. Similar fluctuations in hydrogen absorption capacity have

**Table 5 – The hydrogen capacity and apparent activation energy for some intermetallic hydride.**

| | Intermetallic alloy | | Maximum hydrogen capacity (wt%) | Apparent activation energy ($kJmol^{-1}$) | Ref. |
|---|---|---|---|---|---|
| Very stable hydride | $Zr_{0.9}Ti_{0.4}V_{1.7}$ | | 2.7 (at 298k) | 4.56 | [45] |
| | $A_2B$ hydrides | $Zr_2(Co_{0.5}Fe_{0.2}Ni_{0.2}V_{0.1})$ | 2.1 (at 273k) | 10.11 | This study |
| | | $Zr_2Ni$ | 1.94 | 12.48, 21.02 and 32.98 in three stage of kinetic reaction | [8] |
| | | $Zr_2Fe$ | 1.88 | – | [24] |
| Standard hydride | $LaNi_5$ | | ~1.4 | 27.7 | [46] |
| Are Stable hydride | $(Zr_{0.7}Ti_{0.3})_{1.04}Fe_{1.8}V_{0.2}$ | | 1.51 (at 273k) | 34.5 | [47] |
| | $(Ti_{0.85}Zr_{0.15})_{1.1}Cr_{0.925}MnFe_{0.075}$ | | 1.54 | 52.9 | [48] |
| | $MgH_2$ | | ~4 | 158 | [49] |

Please cite this article as: Komeili M et al., Structural and hydrogen absorption/desorption properties of $Zr_2(Co_{0.5}Fe_{0.2}Ni_{0.2}V_{0.1})$ intermetallic alloy, International Journal of Hydrogen Energy, https://doi.org/10.1016/j.ijhydene.2021.03.045

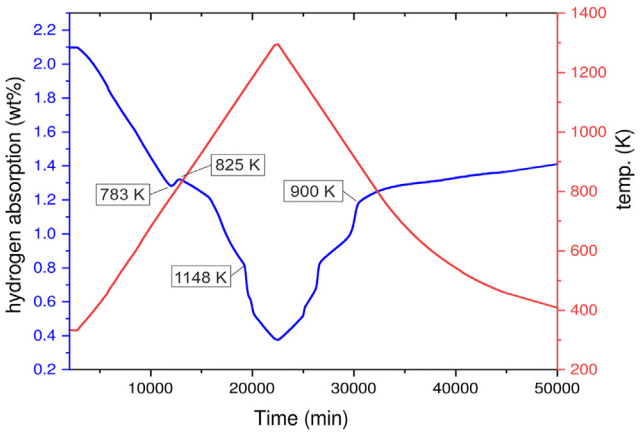


**Fig. 13 – The temperature-programmed hydrogen desorption of $Zr_2(Co_{0.5}Fe_{0.2}Ni_{0.2}V_{0.1})$ alloy.**

been reported for binary alloys $Zr_2Co$, $Zr_2Fe$, and $Zr_2Ni$ at 760, 800, and 840 K, respectively [20]. A significant change in the slope of hydrogen capacity is observed at 973 K, which is related to the formation of the $ZrCo_2$ phase [22]. At higher temperatures up to 1300 K, some other reactions took place that can be seen from the change in the slope curve of hydrogen capacity. These reactions probably are related to the re-disproportionation reaction [20].

By increasing temperature from 1148 to 1300 K and vice versa, it is noticeable that the curve has a symmetric behavior. This means, all the reactions that take place in the hydrogen desorption part (heating stage), are reversed at the same temperature with an equal rate in the hydrogen reabsorption part (cooling stage). Therefore, in this part of the diagram, no unwanted reactions have occurred. In other words, the reactions in this area are related to decomposition of the stable phases and their re-formation, respectively. In the cooling stage, after 900 K, the slope of the hydrogen uptake decreases significantly. Probably hydrogen absorption and disproportionation reaction occur simultaneously during the cooling process. As a result, after cooling the sample to room temperature, the amount of hydrogen absorbed in the sample is lower than that of the initial point.

## Conclusion

Here, for the first time, we have synthesized the $Zr_2(Co_{0.5}Fe_{0.2}Ni_{0.2}V_{0.1})$ intermetallic alloy by arc melting method. It was found that it is a good storage material, which is absorbed hydrogen and, perhaps, its isotopes at ambient conditions.

The following results were obtained from this study:

1. structural analyses of the $Zr_2(Co_{0.5}Fe_{0.2}Ni_{0.2}V_{0.1})$ alloy show a multiphase structure, that the dominant phases are $Zr_2M$, (M = Co, Ni, Fe, or combination of them), which are in agreement with the results determined by Mössbauer spectroscopy.
2. The effect of heating temperature, time of heating, and applied pressure on the activation process examined. It was found that the optimum activation time is 2 h, and the optimum pressure is about 2.65 bar.
3. This alloy has a high hydrogen absorption kinetics rate (saturation time is less than 30 s), and high hydrogen capacity of about 2.1 wt% at room temperature in the first hydrogen cycle. The mechanism of hydrogen kinetic reaction in this alloy is the second-order reaction and its activation energy is found to be 10.11 kJ/mol.
4. The amount of hydrogen stored in the alloy decreases significantly (about 25%) in the first to third absorption/desorption cycles and then becomes almost constant. The stability of hydrogen capacity and the absence of $Zr_2M$ (M = Co, Ni, and Fe) phases indicating that $Zr_2(Co_{0.5}Fe_{0.2}Ni_{0.2}V_{0.1})$ alloy has a good anti-disproportionation property. Hydrogen-induced disproportionation took placed at a temperature of 783 K.

## Declaration of competing interest

The authors declare that they have no known competing financial interests or personal relationships that could have appeared to influence the work reported in this paper.

## Acknowledgement

The work was supported by Ferdowsi University of Mashhad (Grand no. 3/43498).

## REFERENCES

[1] Sakintuna B, Lamari-Darkrim F, Hirscher M. Metal hydride materials for solid hydrogen storage: a review. Int J Hydrogen Energy 2007;32:1121–40. https://doi.org/10.1016/j.ijhydene.2006.11.022.
[2] Liu W, Webb CJ, Gray EMA. Review of hydrogen storage in AB3 alloys targeting stationary fuel cell applications. Int J Hydrogen Energy 2016;41:3485–507. https://doi.org/10.1016/j.ijhydene.2015.12.054.
[3] Bhatnagar A, Gupta BK, Tripathi P, Veziroglu A, Hudson MSL, Shaz MA, et al. Development and demonstration of air stable rGO-EC@AB 5 type hydrogenated intermetallic hybrid for hydrogen fuelled devices. Adv Sustain Syst 2017;1:1700087. https://doi.org/10.1002/adsu.201700087.
[4] hsiung Young K, Nei J. The current status of hydrogen storage alloy development for electrochemical applications. Materials (Basel) 2013;6:4574–608. https://doi.org/10.3390/ma6104574.
[5] Chen XY, Wei LX, Deng L, Yang FS, Zhang ZX. A review on the metal hydride based hydrogen purification and separation technology. Appl Mech Mater 2014;448–453:3027–36. https://doi.org/10.4028/www.scientific.net/AMM.448-453.3027.
[6] Rusman NAA, Dahari M. A review on the current progress of metal hydrides material for solid-state hydrogen storage applications. Int J Hydrogen Energy 2016;41:12108–26. https://doi.org/10.1016/j.ijhydene.2016.05.244.
[7] Bhuiya MMH, Kumar A, Kim KJ. Metal hydrides in engineering systems, processes, and devices: a review of non-storage applications. Int J Hydrogen Energy

2015;40:2231–47. https://doi.org/10.1016/j.ijhydene.2014.12.009.
[8] Ruz P, Sudarsan V. An investigation of hydriding performance of Zr2-xTixNi (x = 0.0, 0.3, 0.7, 1.0) alloys. J Alloys Compd 2015;627:123–31. https://doi.org/10.1016/j.jallcom.2014.12.094.
[9] Coleman M, Chandra D, Wermer J, Udovic TJ. Zirconium iron disproportionation during hydriding reactions in nuclear gettering operations. Adv Mater Energy Convers II 2004:429–35.
[10] Wang F, Li R, Ding C, Tang W, Wang Y, Xu S, et al. Recent progress on the hydrogen storage properties of ZrCo-based alloys applied in International Thermonuclear Experimental Reactor (ITER). Prog Nat Sci Mater Int 2017;27:58–65. https://doi.org/10.1016/j.pnsc.2016.12.018.
[11] Ferreira MJ, Seraphim RM, Ramirez AJ, Tabacniks MH, Nascente PAP. Characterization and evaluation of Ti-Zr-V non-evaporable getter films used in vacuum systems. Phys Procedia 2012;32:840–52. https://doi.org/10.1016/j.phpro.2012.03.644.
[12] Wang F, Li R, Ding C, Wan J, Yu R, Wang Z. Effect of catalytic Ni coating with different depositing time on the hydrogen storage properties of ZrCo alloy. Int J Hydrogen Energy 2016;41:17421–32. https://doi.org/10.1016/j.ijhydene.2016.07.077.
[13] Jat RA, Parida SC, Agarwal R, Kulkarni SG. Effect of Ni content on the hydrogen storage behavior of ZrCo 1-xNix alloys. Int J Hydrogen Energy 2013;38:1490–500. https://doi.org/10.1016/j.ijhydene.2012.11.053.
[14] Jat RA, Singh R, Parida SC, Das A, Agarwal R, Mukerjee SK, et al. Structural and hydrogen isotope storage properties of Zr-Co-Fe alloy. Int J Hydrogen Energy 2015;40:5135–43. https://doi.org/10.1016/j.ijhydene.2015.02.094.
[15] Wan J, Li R, Wang F, Ding C, Yu R, Wu Y. Effect of Ni substitution on hydrogen storage properties of Zr0.8Ti0.2Co1-xNix (x = 0, 0.1, 0.2, 0.3) alloys. Int J Hydrogen Energy 2016;41:7408–18. https://doi.org/10.1016/j.ijhydene.2016.03.112.
[16] Yang G, Liu W, Han X, Han H, Qian Y, Zeng Y, et al. Effects of alloying substitutions on the anti-disproportionation behavior of ZrCo alloy. Int J Hydrogen Energy 2017;42:15782–9. https://doi.org/10.1016/j.ijhydene.2017.05.054.
[17] Kumar S, Tiwari GP, Sonak S, Jain U, Krishnamurthy N. High performance FeTi - 3.1 mass % V alloy for on board hydrogen storage solution. Energy 2014;75:520–4. https://doi.org/10.1016/j.energy.2014.08.011.
[18] Han L, Huang H, Zhang P, Ma C, Wang X, Sang G, et al. Hydrogen storage properties of Zr2Co crystalline and amorphous alloys. Int J Hydrogen Energy 2020. https://doi.org/10.1016/j.ijhydene.2020.10.051.
[19] Guo X, Wang S, Liu X, Li Z, Ye J, Yuan H, et al. Structural characteristics and mechanism of hydrogen-induced disproportionation of the ZrCo alloy. Int J Miner Metall Mater 2012;19:1010–5. https://doi.org/10.1007/s12613-012-0662-7.
[20] Hara M, Hayakawa R, Kaneko Y, Watanabe K. Hydrogen-induced disproportionation of Zr2M (M = Fe, Co, Ni) and reproportionation. J Alloys Compd 2003;352:218–25. https://doi.org/10.1016/S0925-8388(02)01169-6.
[21] Fokin VN, Fokina EE, Tarasov BP. Hydrogenation of the intermetallic compound Zr2Ni. Inorg Mater 2014;50:19–22. https://doi.org/10.1134/S0020168514010063.
[22] Hara M, Hayakawa R, Watanabe K. Hydrogen-induced disproportionation of Zr2Co, vol. 41. Japan Inst of Metals; 2000. https://doi.org/10.2320/matertrans1989.41.1146.
[23] Pitt MP, Pitt LKW, Fjellvg H, Hauback BC. An in situ neutron diffraction study of the thermal disproportionation of the Zr2FeD5 system. J Alloys Compd 2011;509:5515–24. https://doi.org/10.1016/j.jallcom.2011.02.129.
[24] Song J, Wang J, Hu X, Meng D, Wang S. Activation and disproportionation of Zr2Fe alloy as hydrogen storage material. Molecules 2019;24:1542. https://doi.org/10.3390/molecules24081542.
[25] Huot J, Akiba E, Ishido Y. Crystal structure of multiphase alloys (Zr,Ti)(Mn,V)2. J Alloys Compd 1995;231:85–9. https://doi.org/10.1016/0925-8388(95)01842-5.
[26] Rodríguez-Carvajal J. Recent advances in magnetic structure determination by neutron powder diffraction. Phys B Phys Condens Matter 1993;192:55–69. https://doi.org/10.1016/0921-4526(93)90108-I.
[27] Liu XJ, Zhang HH, Wang CP, Ishida K. Experimental determination and thermodynamic assessment of the phase diagram in the Co-Zr system. J Alloys Compd 2009;482:99–105. https://doi.org/10.1016/j.jallcom.2009.04.032.
[28] Stein F, Sauthoff G, Palm M. Experimental determination of intermetallic phases, phase equilibria, and invariant reaction temperatures in the Fe-Zr system. J Phase Equil 2002;23:480–94. https://doi.org/10.1361/105497102770331172.
[29] Okamoto H, Schlesinger ME, Mueller EM. Binary alloy phase diagrams. 2nd ed. ASM International. ASM International; 2016.
[30] Raj P, Suryanarayana P, Sathyamoorthy A, Shashikala K, Iyer RM. Zr2FeHx system hydrided at low temperatures: structural aspects by Mössbauer and x-ray diffraction studies. J Alloys Compd 1992;178:393–401. https://doi.org/10.1016/0925-8388(92)90280-M.
[31] Filippov VP, Bateev AB, Lauer YA, Kargin NI. Mössbauer spectroscopy of zirconium alloys. Hyperfine Interact 2013;217:45–55. https://doi.org/10.1007/s10751-012-0747-8.
[32] Ramos CP, Granovsky MS, Saragovi C. Mössbauer spectroscopy characterization of Zr-Nb-Fe phases. Phys B Condens Matter 2007;389:67–72. https://doi.org/10.1016/j.physb.2006.07.026.
[33] Ostrasz A. Creation of ferromagnetic properties of V-Fe and Zr-Fe alloys by hydrogen absorption. Hyperfine Interact 2006;169:1247–51. https://doi.org/10.1007/s10751-006-9432-0.
[34] Sawicki JA. Iron-bearing precipitates in Zircaloys: a Mössbauer spectroscopy study. J Nucl Mater 1996;228:238–47. https://doi.org/10.1016/S0022-3115(95)00196-4.
[35] Devillers M, Sirch M, Bredendiek-Kämper S, Penzhorn RD. Characterization of the ZrCo-hydrogen system in view of its use for tritium storage. Chem Mater 1990;2:255–62. https://doi.org/10.1021/cm00009a014.
[36] Zalkind S, Nahmani M, Shamir N. The interaction of Zr2Fe surface with O2 and H 2O at the temperature range 300-770 K. J Alloys Compd 2010;501:221–6. https://doi.org/10.1016/j.jallcom.2010.01.165.
[37] Zhang Y, Li J, Zhang T, Kou H, Xue X. Hydrogen absorption properties of a non-stoichiometric Zr-based Laves alloy against gaseous impurities. Int J Hydrogen Energy 2017;42:10109–16. https://doi.org/10.1016/j.ijhydene.2017.02.040.
[38] Cekić B, Ćirić K, Iordoc M, Marković S, Mitrić M, Stojić D. Kinetics of hydrogen absorption in Zr-based alloys. J Alloys Compd 2013;559:162–6. https://doi.org/10.1016/j.jallcom.2013.01.104.
[39] Li SL, Wang P, Chen W, Luo G, Chen DM, Yang K. Effect of non-stoichiometry on hydrogen storage properties of La(Ni3.8Al1.0Mn0.2)x alloys. Int J Hydrogen Energy 2010;35:3537–45. https://doi.org/10.1016/j.ijhydene.2010.01.102.
[40] Peng L, Jiang C, Xu Q, Wu X. Hydrogen-induced disproportionation characteristics of Zr(1-x)Hf(x)Co(x = 0,

Please cite this article as: Komeili M et al., Structural and hydrogen absorption/desorption properties of $Zr_2(Co_{0.5}Fe_{0.2}Ni_{0.2}V_{0.1})$ intermetallic alloy, International Journal of Hydrogen Energy, https://doi.org/10.1016/j.ijhydene.2021.03.045

0.1, 0.2 and 0.3) alloys. Fusion Eng Des 2013;88:299–303. https://doi.org/10.1016/j.fusengdes.2013.03.027.
[41] Zhang TB, Wang XF, Hu R, Li JS, Yang XW, Xue XY, et al. Hydrogen absorption properties of Zr(V1-xFex) 2 intermetallic compounds. Int J Hydrogen Energy 2012;37:2328–35. https://doi.org/10.1016/j.ijhydene.2011.10.089.
[42] Pang Y, Li Q. A review on kinetic models and corresponding analysis methods for hydrogen storage materials. Int J Hydrogen Energy 2016;41:18072–87. https://doi.org/10.1016/j.ijhydene.2016.08.018.
[43] Atilio Puszkiel J. Tailoring the kinetic behavior of hydride forming materials for hydrogen storage. Gold nanoparticles - reach new height. https://doi.org/10.5772/intechopen.82433; 2019.
[44] Khawam A, Flanagan DR. Solid-state kinetic models: basics and mathematical fundamentals. J Phys Chem B 2006;110:17315–28. https://doi.org/10.1021/jp062746a.
[45] Zhang Y, Li J, Zhang T, Wu T, Kou H, Xue X. Hydrogenation thermokinetics and activation behavior of non-stoichiometric Zr-based Laves alloys with enhanced hydrogen storage capacity. J Alloys Compd 2017;694:300–8. https://doi.org/10.1016/j.jallcom.2016.10.021.
[46] Muthukumar P, Satheesh A, Linder M, Mertz R, Groll M. Studies on hydriding kinetics of some La-based metal hydride alloys. Int J Hydrogen Energy 2009;34:7253–62. https://doi.org/10.1016/j.ijhydene.2009.06.075.
[47] Cao Z, Ouyang L, Wang H, Liu J, Sun L, Felderhoff M, et al. Development of Zr-Fe-V alloys for hybrid hydrogen storage system. Int J Hydrogen Energy 2016;41:11242–53. https://doi.org/10.1016/j.ijhydene.2016.04.083.
[48] Cao Z, Ouyang L, Wang H, Liu J, Sun L, Zhu M. Composition design of Ti – Cr – Mn – Fe alloys for hybrid high-pressure metal hydride tanks. J Alloys Compd 2015;639:452–7. https://doi.org/10.1016/j.jallcom.2015.03.196.
[49] Ouyang LZ, Yang XS, Zhu M, Liu JW, Dong HW, Sun DL, et al. Enhanced hydrogen storage kinetics and stability by synergistic. J Phys Chem C 2014;118:7808–20.

Please cite this article as: Komeili M et al., Structural and hydrogen absorption/desorption properties of $Zr_2(Co_{0.5}Fe_{0.2}Ni_{0.2}V_{0.1})$ intermetallic alloy, International Journal of Hydrogen Energy, https://doi.org/10.1016/j.ijhydene.2021.03.045